*Int. J. Multiphase Flow* Vol. 13, No. 5, pp. 583–603, 1987
Printed in Great Britain. 

0301-9322/87 $3.00 + 0.00


# INTERFACIAL INSTABILITIES FOR HORIZONTAL GAS–LIQUID FLOWS IN PIPELINES

N. ANDRITSOS and T. J. HANRATTY
University of Illinois, Urbana, IL 61801, U.S.A.

(*Received* 6 *August* 1985; *in revised form* 15 *October* 1986)

**Abstract**—Experiments were conducted with air and liquid flowing in horizontal pipelines, 2.52 and 9.53 cm dia, to determine the interfacial instabilities that exist in a stratified flow. The liquid viscosity was varied from 1 to 80 cP. Three types of instabilities are defined: regular 2-D waves are associated with pressure variations in phase with the wave slope, irregular large-amplitude waves and atomization of the liquid are associated with pressure variations in phase with the wave height. Linear stability theory is used to provide a physical interpretation and to predict conditions for the initiation of these instabilities.

## 1. INTRODUCTION

At low flows of gas and liquid in a horizontal pipeline a stratified regime exists whereby the liquid moves along the bottom of the pipe and the gas, concurrently with it. Although this pattern can be considered the simplest one for gas–liquid flows, large differences are observed between measurements and presently available correlations for pressure drop and hold-up. The main reason is that waves can cause the drag of the gas on the liquid to be greater than if the interface were smooth. This causes larger pressure drops and smaller hold-ups than are predicted if the Blasius equation is used to calculate the interfacial stress.

This problem is recognized in flow maps (Baker 1954; Mandhane *et al.* 1974; Taitel & Dukler 1976a) by the definition of smooth-stratified and wavy-stratified patterns. However, these maps have shortcomings since they do not accurately characterize the type of waves and since the suggested transitions do not reflect observed effects of changes of liquid viscosity and of pipe diameter.

Most of the studies of wave generation in concurrent gas–liquid flows have been conducted for rectangular channels with a large aspect ratio (Hanratty & Engen 1957; Hanratty & Hershman 1961; Hanratty 1983). For air–water flows no waves are observed at sufficiently low gas velocities. The first waves observed with increasing gas velocity are 2-D capillary–gravity waves. These appear to be unstable to 3-D disturbances, so that they exist over a narrow range of gas velocities. The 3-D waves have a pebbled appearance and characteristic wavelengths which decrease with increasing gas velocity. At sufficiently high gas velocities, long-wavelength large-amplitude waves with a highly roughened interface appear. These "roll waves" carry large masses of fluid and may actually be looked upon as flow surges in the liquid layer. At very high gas velocities atomization occurs through the removal, by the gas, of wavelets riding on the top of the roll waves.

One of the main theoretical problems in interpreting these results is the prediction of the spatial variation of the gas-phase pressure and shear stress induced at the interface by the presence of the waves. The principal theoretical tool has been linear stability theory. A summary of progress in this direction is given in a recent review article by Hanratty (1983). The 2-D and pebbled waves are interpreted as resulting from an imbalance between the energy fed to the waves by wave-induced pressure variations in phase with the wave slope and viscous dissipation. Roll waves occur when the destabilizing effects of liquid inertia and long-wavelength pressure variations in phase with the wave height overcome the stabilizing effect of gravity. Atomization is suggested to be the result of an imbalance between the destabilizing effect of pressure variations over small-wavelength waves and the stabilizing effect of surface tension.

The objective of this paper is to characterize the different types of wave patterns observed for gas–liquid flow in a horizontal circular pipe. The results are interpreted using theoretical approaches already applied to channel flows. Particular emphasis is placed on the prediction of the effect of changes of liquid viscosity and of pipe diameter.

## 2. THEORY

### (a) *Definitions of the problem*

The observed transitions are interpreted by examining the conditions under which small-amplitude sinusoidal waves will grow or decay. It is recognized that this approach has limitations since not all of the observed interfacial structures originate from the growth of small disturbances. A more complete description would require the consideration of non-linear effects.

In order to simplify the analysis, the 2-D system shown in figure 1 is considered. The flow is assumed to be steady. The average velocities in the liquid and gas are designated by $U_L$ and $U_G$ and the average height of the liquid, by $\bar{h}$.

A disturbance $h' = h - \bar{h}$ of the following form is introduced at the interface:

$$h' = \hat{h} \exp[ik(x - Ct)], \tag{1}$$

with $x$ being the distance in the direction of flow and $t$, the time. The amplitude, $\hat{h}$, and the wavenumber, $k = 2\pi/\lambda$, are considered to be real. The wave velocity is complex,

$$C = C_R + iC_I. \tag{2}$$

The wave will grow or decay in time depending on the sign of $C_I$. The condition $C_I = 0$ defines neutral stability. The calculations give the conditions ($U_L$, $U_G$, $\bar{h}$) for which $C_I$ is positive and for which the disturbance is growing the fastest ($kC_I$ is a maximum).

### (b) *Influence of wave-induced variations of interfacial stresses*

The presence of the waves induces flow disturbances in the gas. These give rise to pressure and shear stress variations at the interface, which can feed or extract energy from the disturbance. The waves are considered to be of small enough amplitude that a linear response is obtained, whereby

$$\frac{\tau_i'}{\hat{\tau}_i} = \frac{P_i'}{\hat{P}_i} = \exp[ik(x - Ct)]. \tag{3}$$

The amplitudes, $\hat{\tau}_i$ and $\hat{P}_i$ are complex and linearly dependent on $\hat{h}$,

$$\hat{\tau}_i = \hat{\tau}_{iR} + i\hat{\tau}_{iI} \tag{4}$$

and

$$\hat{P}_i = \hat{P}_{iR} + i\hat{P}_{iI}. \tag{5}$$

The real parts of [4] and [5] can be written as

$$\tau_i' = \hat{\tau}_{iR} \cos k(x - Ct) - \hat{\tau}_{iI} \sin k(x - Ct), \tag{6}$$

and

$$P_i' = \hat{P}_{iR} \cos k(x - Ct) - \hat{P}_{iI} \sin k(x - Ct). \tag{7}$$

Thus $\hat{\tau}_{iR}$ and $\hat{P}_{iR}$ are the amplitudes of components in phase with the wave height and $-\hat{\tau}_{iI}$ and $-\hat{P}_{iI}$ are the amplitudes of components in phase with the wave slope.

The velocity field in the liquid is given as

$$u_x = \bar{u} + u_x' \tag{8}$$

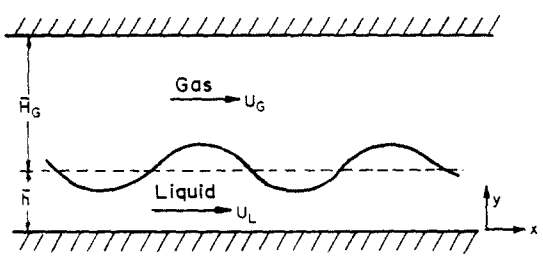


Figure 1. System to which stability analysis is applied.

and

$$u_y = u'_y. \qquad [9]$$

The gas-phase pressure field feeds energy to the liquid by coupling with velocity component $u'_y$. A negative $\hat{P}_{iR}$ is destabilizing since it gives a suction at the crest where $u'_y$ is positive and a compression at the trough where $u'_y$ is negative. This causes, what is called, a Kelvin–Helmholtz instability. Similarly, the destabilizing effect of a positive $\hat{P}_{iI}$ is associated with the sheltering mechanism for wave generation, described by Jeffreys (1925).

The gas-phase shear stress field feeds energy into the liquid through velocity component $u'_x$ and is destabilizing for positive $\tau_{iR}$ or negative $\hat{\tau}_{iI}$. Because of the small gas viscosity $\tau'_i$ is usually much smaller than $P'_i$. One can, therefore, expect $\tau'_i$ to play an important role in wave generation only for thin films for which $u'_x \gg u'_y$.

*(c) Stability analysis*

The spatial and temporal variation of $u'_x$ and $u'_y$ are defined by the linear momentum balance equations for the liquid since $u'_x$ and $u'_y$ are considered small compared to $\bar{u}$. The solution of these equations is complicated because of the variation of $\bar{u}$ with $y$. Consequently, it is difficult to obtain results valid for a wide range of Reynolds numbers and of $(\bar{u} - C_R)$. This difficulty will be avoided by assuming a plug flow in the liquid, with a velocity of $U_L$. The main limitation of the solutions is that they do not correctly describe situations where the wavelength, $\lambda$, is very large compared to the height of the liquid layer, $\bar{h}$. These cases are best considered by using integral forms of the momentum equations (Hanratty 1983). Consequently the solutions developed by Lin & Hanratty (1986) will be used when $\lambda \gg \bar{h}$ and $\lambda \gg \bar{H}$.

The equations describing $u'_x$ and $u'_y$ are, therefore, given as

$$\frac{\partial u'_x}{\partial t} + U_L \frac{\partial u'_x}{\partial x} = -\frac{1}{\rho_L}\frac{\partial p'}{\partial x} + \nu_L\left(\frac{\partial^2 u'_x}{\partial x^2} + \frac{\partial^2 u'_x}{\partial y^2}\right), \qquad [10]$$

$$\frac{\partial u'_y}{\partial t} + U_L \frac{\partial u'_y}{\partial x} = -\frac{1}{\rho_L}\frac{\partial p'}{\partial y} + \nu_L\left(\frac{\partial^2 u'_y}{\partial x^2} + \frac{\partial^2 u'_y}{\partial y^2}\right) - g \qquad [11]$$

and

$$\frac{\partial u'_x}{\partial x} + \frac{\partial u'_y}{\partial y} = 0. \qquad [12]$$

These are solved under the conditions that $u'_x$ and $u'_y$ vanish at $y = 0$ and that the stresses in the liquid at the interface, $\sigma_{yx}$ and $\sigma_{yy}$, equal the stresses in the gas, $\tau_i$ and $P_i$:

$$\sigma'_{yx} = \tau'_i, \qquad [13]$$

and

$$\sigma'_{yy} = P_\sigma + P'_i, \qquad [14]$$

with

$$\sigma'_{yx} = \mu_L\left(\frac{\partial u'_x}{\partial y} + \frac{\partial u'_y}{\partial x}\right), \qquad [15]$$

$$\sigma'_{yy} = -p' + 2\mu_L \frac{\partial u'_y}{\partial y} \qquad [16]$$

and

$$P_\sigma = \sigma \frac{\partial^2 h'}{\partial x^2}. \qquad [17]$$

These are solved by the methods outlined by Lamb (1945), Levich (1962) and Taylor (1963). The solutions to [10]–[12] are given as

$$u'_x = -\frac{\partial \phi}{\partial x} - \frac{\partial \psi}{\partial y}, \qquad [18]$$

$$u'_y = -\frac{\partial \phi}{\partial y} + \frac{\partial \psi}{\partial x} \tag{19}$$

and

$$\frac{p'}{\rho_L} = \frac{\partial \phi}{\partial t} - U_L \frac{\partial \phi}{\partial x} - g(y - \bar{h}), \tag{20}$$

provided

$$\frac{\partial^2 \phi}{\partial x^2} + \frac{\partial^2 \phi}{\partial y^2} = 0 \tag{21}$$

and

$$\frac{\partial \psi}{\partial t} + U_L \frac{\partial \psi}{\partial x} = \nu_L \left[ \frac{\partial^2 \psi}{\partial x^2} + \frac{\partial^2 \psi}{\partial y^2} \right]. \tag{22}$$

The solutions of [21] and [22] are taken as

$$\phi = [A \sinh(ky) + B \cosh(ky)] \exp[ik(x - Ct)] \tag{23}$$

and

$$\psi = [D \cosh(ly) + E \sinh(ly)] \exp[ik(x - Ct)], \tag{24}$$

with

$$l^2 = k^2 - \frac{ik(C - U_L)}{\nu_L}. \tag{25}$$

The requirement of zero velocity at $y = 0$ gives

$$A = iD, \quad B = i\frac{l}{k} E. \tag{26}$$

Boundary conditions [13] and [14] and the kinematic condition at the interface,

$$\frac{\partial h'}{\partial t} + U_L \frac{\partial h'}{\partial x} = u'_y @ y = \bar{h}, \tag{27}$$

define constants D and E and provide the following relation between $k$ and $C$:

$$k\bar{h}(C - U_L)^2 \frac{\dfrac{-2lk + \hat{\tau}_c \dfrac{l}{k}}{\sinh(k\bar{h}) \sinh(l\bar{h})} + (l^2 + k^2 + \hat{\tau}_c)\left[\dfrac{l}{k} \coth(k\bar{h}) \coth(l\bar{h}) - 1\right]}{(l^2 - k^2)\left[\dfrac{l}{k} \coth(l\bar{h}) - \coth(k\bar{h})\right]}$$

$$+ i2\frac{\nu_L}{\bar{h}} (k\bar{h})^2 (C - U_L) \left\{ \frac{\dfrac{-\dfrac{l}{k}\left[(2k^2 - \hat{\tau}_c) + (l^2 + k^2 - \hat{\tau}_c)\right]}{\sinh(k\bar{h}) \sinh(l\bar{h})}}{(l^2 - k^2)\left[\dfrac{l}{k} \coth(l\bar{h}) - \coth(k\bar{h})\right]} \right.$$

$$\left. \frac{-\left[(l^2 + k^2 - \hat{\tau}_c) + \dfrac{l^2}{k^2}(2k^2 - \hat{\tau}_c)\right] + \dfrac{l}{k}\left[(2k^2 - \hat{\tau}_c) + (l^2 + k^2 - \hat{\tau}_c)\right] \coth(k\bar{h}) \coth(l\bar{h})}{(l^2 - k^2)\left[\dfrac{l}{k} \coth(l\bar{h}) - \coth(k\bar{h})\right]} \right\}$$

$$= \frac{\bar{h}}{\rho_L}\left[k^2\sigma + (\rho_L - \rho_G)g + \frac{\hat{P}_i}{\hat{h}}\right], \tag{28}$$

where

$$\tau_c = \frac{\left(\frac{\hat{\tau}_i}{\hat{h}}\right)}{\mu_L(C - U_L)}. \qquad [29]$$

By separately equating the real and imaginary parts of [28] to zero, two equations defining $C_R$ and $C_I$ are obtained.

Cohen & Hanratty (1965) and Craik (1968) derived an equation similar to [28]. They did not assume $\bar{u}(y)$ is described by a plug flow and present a solution to [10]–[12] which is valid for large liquid Reynolds numbers. Equation [4.8] from Craik's paper is identical to [28] at large Reynolds number, if the surface contamination terms in Craik's result are ignored.

*(d) Estimation of the surface stresses*

The principal problem in calculating $C_R$ and $C_I$ from [28] is the specification of $\hat{P}_{iR}$, $\hat{P}_{iI}$, $\hat{\tau}_{iR}$ and $\hat{\tau}_{iI}$. These are obtained by solving momentum balance equations for the gas, which are linearized around an average velocity profile. If this profile is assumed to be a plug flow and if viscous effects are neglected,

$$\frac{\hat{P}_{iR}}{\hat{h}} = -\frac{k\bar{H}}{\tanh(k\bar{H})}\frac{\rho_G}{\bar{H}}(U_G - C)^2 \qquad [30]$$

and

$$\hat{P}_{iI} = \hat{\tau}_{iR} = \hat{\tau}_{iI} = 0. \qquad [31]$$

In addition, if $k\bar{H} \to 0$,

$$\frac{\hat{P}_{iR}}{\hat{h}} = -\frac{\rho_G}{\bar{H}}(U_G - C)^2. \qquad [32]$$

The inclusion of viscous effects and the linearization around a measured velocity profile for flow over a flat plate gives more realistic results, with non-zero values of $\hat{P}_{iI}$, $\hat{\tau}_{iR}$ and $\hat{\tau}_{iI}$. This paper uses this type solution to evaluate the surface stress terms in [28].

An additional problem arises in formulating the linear momentum equations because the gas flow is turbulent. The presence of waves at the interface induces variations of the Reynolds stresses, which need to be specified. A completely satisfactory method for doing this is not yet available. [See Hanratty (1983) for a summary of progress.]

The solution for $\hat{P}_{iR}$, $\hat{P}_{iI}$, $\hat{\tau}_{iR}$ and $\hat{\tau}_{iI}$ uses a model for the wave-induced Reynolds stresses which does a good job in describing measurements of the shear stress variation along solid wavy walls. This is the Model D* described by Thorsness *et al.* (1978) and by Zilker *et al.* (1977). The method of calculation may be found in the above papers and, in much greater detail, in a recent thesis by Abrams (1984). It is limited to cases for which $\lambda/\bar{H} < 2\pi$.

Lin & Hanratty (1986), in their recent study of the initiation of slugs, used integral methods both for the gas and the liquid, to analyze the stability of the liquid for the case of $\lambda \gg \bar{H}$. Pressure amplitude, $\hat{P}_{iR}$, was calculated using an equation very close to [32]. This solution will be used here, with $\hat{P}_{iR}$ given by [30] instead of [32], for large $\lambda/\bar{H}$.

*(e) Examples of stability calculations*

The stability analysis for a channel was applied to a pipe flow by assuming the liquid layer thickness used in the channel flow calculations is equal to a liquid height defined as the area occupied by the liquid divided by the width of the interface (Chow 1959).

Figures 2 and 3 illustrate the effect of changing the ratio of the height of the liquid along the pipe centerline to the pipe diameter from 0.4 to 0.2. Figure 4 illustrates the effect of increasing the viscosity from 1 to 80 cP. The ordinate in these plots is the wavelength. The abscissa is the superficial gas velocity, calculated as if no liquid were flowing. The average velocity of the liquid was obtained from a momentum balance for a fully developed condition, as outlined by Taitel & Dukler (1976b). The interfacial friction factor was calculated using the Blasius law and the concept of a hydraulic diameter. In actual flows the interfacial friction factor could be larger than predicted

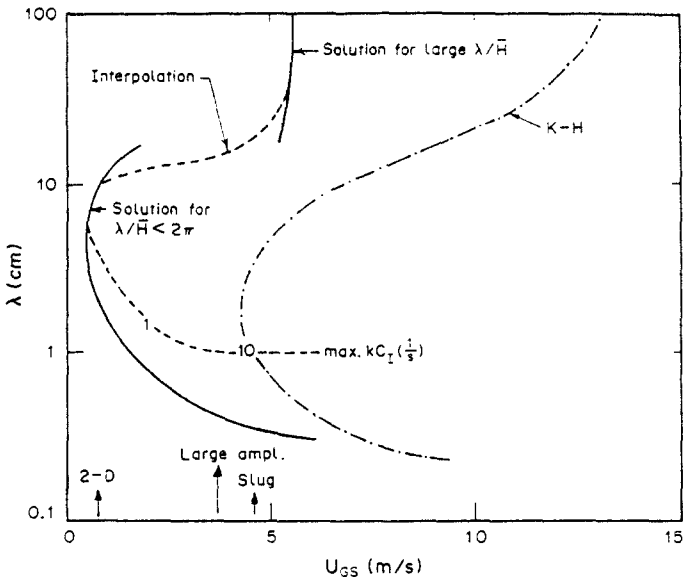


Figure 2. Calculation of neutral stability curve and maximum growth rate locus ($D = 9.53$ cm, $\mu_L = 1$ cP, $\bar{h}/D = 0.4$).

by the Blasius equation because of the existence of a roughened interface. This larger friction factor does not affect appreciably the neutral stability curve or the location of the curve of maximum growth, but it does affect significantly the magnitude of the growth rate.

The solid curve spanning the lower wavelengths is the neutral stability curve (the loci of $C_I = 0$) calculated from [28] for $\lambda/\bar{H} < 2\pi$. The solid curve at large wavelengths is the neutral stability curve calculated from Lin's analysis (which is invalid for small $\lambda$). The dashed curve represents a possible interpolation between these two results. The region inside and to the right of these curves is a region of instability ($C_I > 0$). The conditions for maximum growth are also indicated by the loci of the maxima in $kC_I$.

The results shown in figures 2–4 are essentially unchanged if the conditions $\hat{\tau}_{iR} = \tau_{il} = 0$ are used in the calculations, provided $\lambda$ is not too large. This indicates that only the wave-induced variation of the gas-phase pressure is affecting the calculation of the minimum critical gas velocity and the calculation of the fastest growing wave.

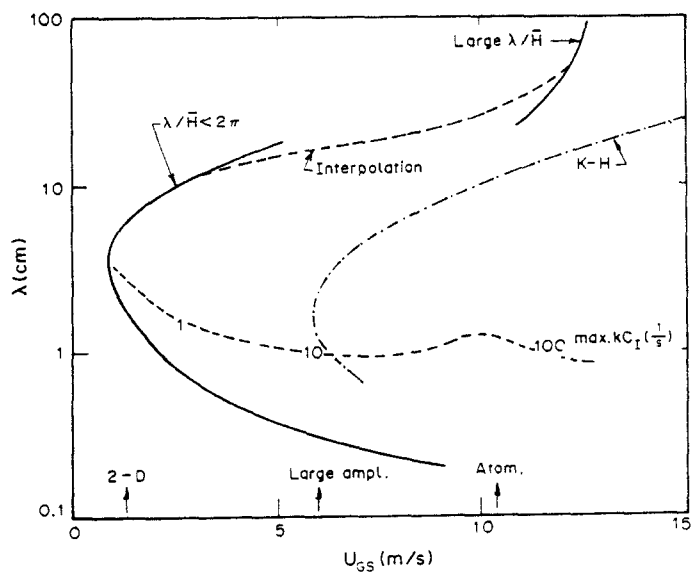


Figure 3. Calculation of neutral stability curve and maximum growth rate locus ($D = 9.53$ cm, $\mu_L = 1$ cP, $\bar{h}/D = 0.2$).

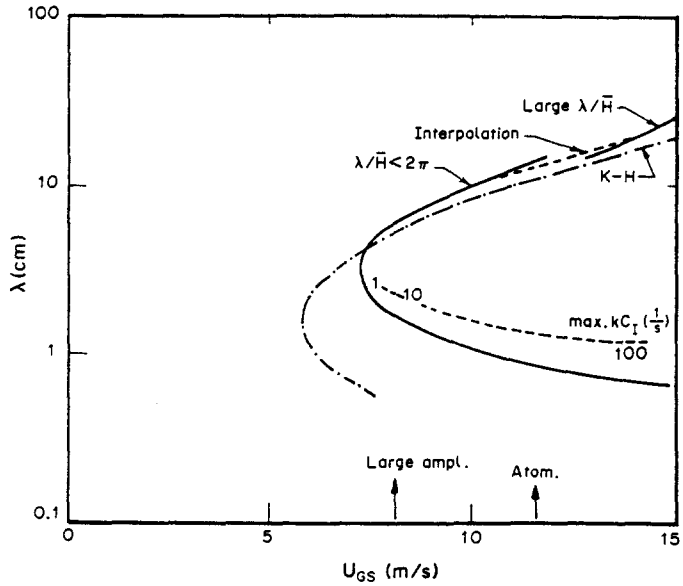


Figure 4. Calculation of neutral stability curve and maximum growth rate locus ($D = 9.53$ cm, $\mu_L = 80$ cP, $\bar{h}/D = 0.2$).

Figure 5 examines the relative importance of $\hat{P}_{il}$ and $\hat{P}_{iR}$ for a water flow. The —— curve presents the maximum values of $kC_I$. The – – – curve is the same calculation with $\hat{P}_{iR} = 0$. The –·– curve is the calculation with $\hat{P}_{il} = 0$. It is noted that $\hat{P}_{iR}$ has no effect on the calculated maxima in $kC_I$ at small gas velocities. This suggests that the critical gas velocity needed to generate waves on water flows is determined completely by a sheltering mechanism, whereby energy is fed to the waves by a pressure component which is in phase with the wave slope. It is also noted that pressure variations in phase with the wave height ($\hat{P}_{iR}$) start to become important at a superficial gas velocity of $U_{GS} \cong 7$ m/s and become dominant at $U_{GS} \cong 9$ m/s.

Very-large-wavelength disturbances are not possible for small gas velocities. However, it is noted that at a certain critical gas velocity, which is strongly dependent on $\bar{h}/D$, the generation of very-large-wavelength waves is possible. Lin & Hanratty (1986) interpret this as the critical condition for the initiation of slugs. In this region all of the interfacial stress components are contributing, but $\hat{P}_{iR}$ is the dominant effect.

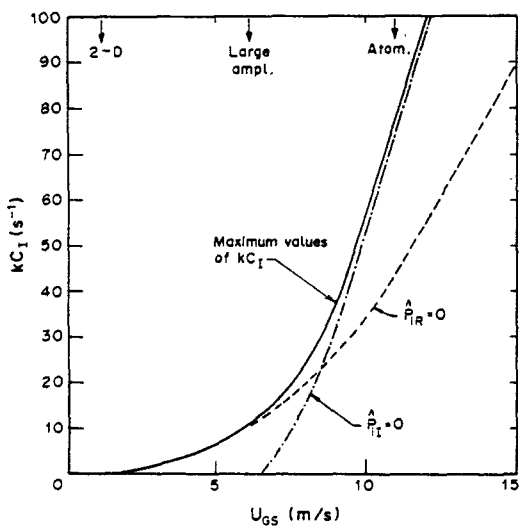


Figure 5. Calculation of growth rate as a function of superficial gas velocity ($D = 9.53$ cm, $\mu_L = 1$ cP, $\bar{h}/D = 0.2$).

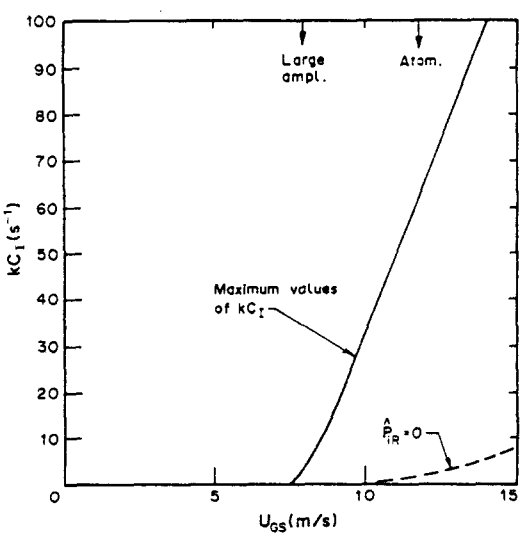


Figure 6. Calculation of growth rate as a function of superficial gas velocity ($D = 9.53$ cm, $\mu_L = 80$ cP, $\bar{h}/D = 0.2$).

The effect of an increase in viscosity can be seen by comparing figures 4 and 6 with figures 3 and 5. As would be expected, the critical velocity necessary to generate waves increases with increasing liquid viscosity. A comparison of figures 5 and 6 for the case of $\hat{P}_{iR} = 0$ indicates that a sheltering hypothesis by itself ($\hat{P}_{iI} \neq 0$, $\hat{P}_{iR} = 0$) would predict the initiation of waves at a gas velocity which is too high. The discrepancy becomes greater with increasing liquid viscosity. This illustrates what had already been pointed out by Francis (1954, 1956) and by Miles (1959) that the initiation of waves on high-viscosity liquids is controlled by a Kelvin–Helmholtz (K–H) mechanism ($\hat{P}_{iR} \neq 0$, $\hat{P}_{iI} = 0$).

The curves in figures 2–4 marked inviscid K–H theory represent calculations that assume inviscid plug flows both in the gas and the liquid. They are obtained using the K–H instability equation:

$$(U_G - \bar{u}_a)^2 \geq [k^2\sigma + (\rho_L - \rho_G)g]\frac{\bar{H}}{\rho_G}\left[\frac{\tanh(k\bar{H})}{k\bar{H}} + \frac{\rho_G}{\rho_L}\frac{\tanh(k\bar{h})}{k\bar{H}}\right]. \quad [33]$$

For the case of water flows, inviscid K–H theory predicts an initiation of waves at gas velocities that are too high. This is because the influence of pressure components in phase with the wave slope is ignored (Jeffreys 1925). For viscous fluids the inviscid K–H theory predicts the initiation of waves at a lower gas velocity than is calculated from the full viscous equations, because it ignores viscous damping in the fluid.

As has already been pointed out by Lin & Hanratty (1986), inviscid K–H theory is found to predict gas velocities for the initiation of large-wavelength waves which are too high (see figure 2). This is because the inviscid theory underestimates the destabilizing effects of inertia in the liquid.

*(f) Effect of pressure*

The effect of gas-phase pressure on the stability calculations is illustrated in figure 7 for the case of a 12 cP liquid flowing in a 9.53 cm pipe. It is noted that the growth rate is approximately independent of pressure if it is plotted against $U_{GS}\sqrt{\rho_G}$. This suggests that the initiation of large-amplitude waves and of atomization will occur at lower gas velocities in high-pressure flows.

It is also noted that the value of $U_{GS}\sqrt{\rho_G}$ needed to initiate regular waves increases with increasing pressure and approaches the value that would be calculated by assuming $\hat{P}_{iI} = 0$. This suggests that the range of gas velocities over which regular waves exist becomes smaller with increasing pressure.

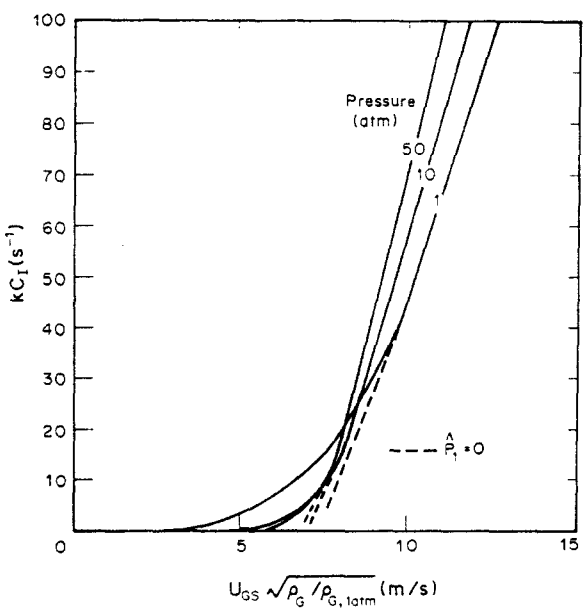


Figure 7. Effect of pressure on growth rate ($\bar{h}/D = 0.2$, $D = 9.53$ cm, $\mu = 12$ cP).

## 3. DESCRIPTION OF THE EXPERIMENTS

The experiments were carried out in the gas–liquid flow system described by Laurinat *et al.* (1984). Tests were made with two Plexiglas sections with i.d.s of 2.52 and 9.53 cm, located 15.5 and 24.6 m from the entry. Studies with high-viscosity fluids in the 2.52 cm pipe were carried out with a smaller test length of 10 m in order to reduce frictional losses. The pipelines were carefully leveled by introducing water into them, closing both ends and adjusting the supports so that the level was the same along the pipeline.

The pipes discharged into a separator which was at atmospheric pressure. A simple pipe tee was used to contact the phases at the entry. The liquid was introduced in the run of the tee and the gas, in the branch.

The liquid viscosity was varied by using solutions of water and glycerine. Solutions with viscosities of 12 and 80 cP were used in the 9.53 cm pipe of 4.5, 16 and 70 cP in the 2.52 cm pipe. Because of limitations in the recirculation pump it was not possible to carry out studies at high liquid velocities with 12 and 80 cP solutions in the 9.53 cm pipe.

The height of the liquid layer was measured by two parallel wire conductance probes that extended over the entire cross section of the pipe. This technique is described by Laurinat *et al.* (1984) and by Lin & Hanratty (1987). For the 9.53 cm pipe, the probe was located 220 pipe diameters from the entrance. For the 2.52 cm pipe, the probe was located 500 pipe diameters from the entrance for water and, 350 pipe diameters for glycerine–water solutions. Wave velocities were measured by locating a second pair of conductance probes 26.7 cm downstream in the 9.53 cm pipe, 25.4 cm downsteam for water flows in the 2.52 cm pipe and 10.2 cm downstream for water–glycerine flows in the 2.52 cm pipe.

Experiments were also carried out in the 9.53 cm pipe in which the liquid layer height was measured 80 and 160 pipe diameters from the entrance. This was done in order to determine the hydraulic gradients that exist at low gas velocities.

## 4. DESCRIPTION OF THE WAVES

### (*a*) *Low-viscosity liquids*

The type of waves observed on a low-viscosity fluid are illustrated by the tracings in figure 8 for a 4.5 cP liquid. For a fixed liquid flow the first waves observed with increasing gas velocity are small-amplitude 2-D waves of wavelength 2–4 cm that can only be observed visually by light reflection from the liquid surface. These disturbances first appear at the downstream end of the pipe. An increase in the gas velocity causes the point of initiation to move upstream. These waves increase in amplitude and in wavelength as they propagate downstream. The troughs of the waves observed in the 9.53 cm pipe were covered with an interference wave pattern of small broad crested capillary waves. This was not the case in the 2.52 cm pipe.

Upon increasing the gas flow rate, the amplitudes of the waves become larger and the wavelength decrease. This is illustrated by comparing the wave tracings in figures 8(a,b). The pebbly wave pattern observed by Hanratty & Engen (1957) was encountered only for water flows in the 9.53 cm pipe. It occurred over a narrow range of flow conditions. A curved wave front was also observed for low liquid velocities in the 9.53 cm pipe.

At high enough gas velocities a "large amplitude" wave with a steep front and a gradually sloping back forms close to the entry. Tracings for this type of wave are shown in figures 9(b,c). These "large-amplitude" waves are less regular than the 2-D waves observed at lower gas velocities. This can be seen from the tracings but it can also be detected from the cross correlations of the film height signals from two locations separated in the flow direction. A maximum in the correlation is observed for a certain time delay. For the 2-D small-amplitude waves this maximum is close to unity. However, its value is $<1$ for the "large-amplitude" waves and continues to decrease with increasing gas velocity. Another signature of the "large-amplitude" waves is that the distribution function for film height has a flatness factor $>3$.

At conditions close to the pseudo-slug transition defined by Lin & Hanratty (1987) a wave pattern similar to the roll waves described by Hanratty & Engen (1957) for gas–liquid flow in a

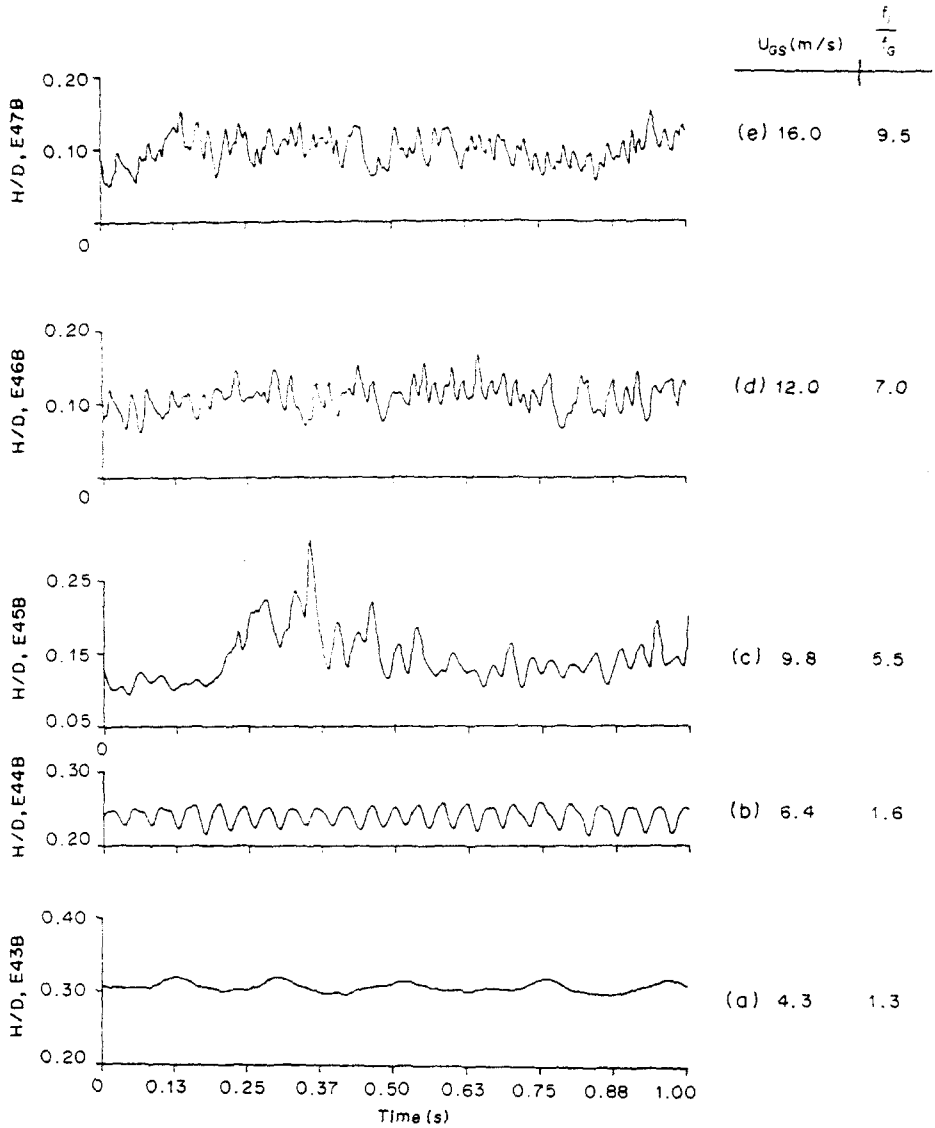


Figure 8. Film thickness tracings for constant superficial liquid velocity ($D = 2.52$ cm, $\mu_L = 4.5$ cP, $U_{LS} = 0.03$ m/s).

channel is observed in the 2.52 cm pipe. In this case, some of the "large-amplitude" waves coalesce to form an even larger accelerating wave. Figure 8(c), or 9(d), gives an example of this type of interfacial disturbance. It is to be noted that it is similar to the "roll wave" observed by Hanratty & Engen (1957) and by Miya *et al.* (1971) in a channel flow.

Above a certain gas velocity the liquid starts to climb up the walls of the pipe and the average shape is no longer approximated by a flat horizontal plane. In addition, droplets or liquid filaments are torn from the liquid phase and deposited on the pipe walls. The initiation of atomization is defined as the gas velocity at which droplets first hit the top of the pipe. At higher gas velocities enough droplets are deposited so that liquid streaks form. This droplet deposition process is the mechanism by which annular flow is initiated in large-diameter pipes (Lin & Hanratty 1987) at gas velocities roughly twice that needed to initiate atomization. Wave wetting can be an additional mechanism for the initiation of annular flow in small-diameter pipes (Lin & Hanratty 1987).

At large gas velocities in the 2.52 cm pipe the large-amplitude waves take the form of aerated ring waves (or disturbances) that wrap around the pipe circumference. For even higher gas velocities (> 100 m/s) these disturbances disappear. In the 9.53 cm pipe they appear as broken pieces of a ring. They do not wrap around the entire circumference until very high gas velocities, say 70 m/s, are reached.

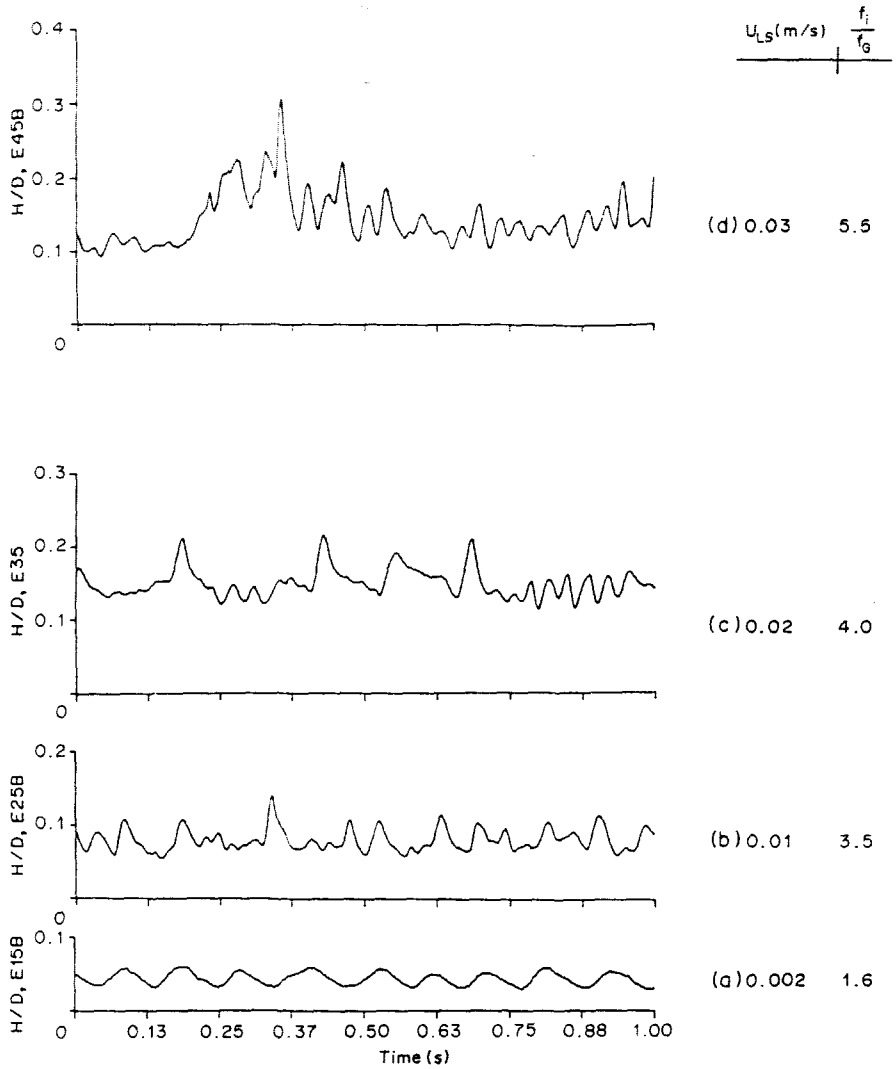


Figure 9. Film thickness tracings for constant superficial gas velocity ($D = 2.52$ cm, $\mu_L = 4.5$ cP, $U_{GS} = 9.8$ m/s).

The flow patterns observed over the range of liquid viscosities of 1–14 cP are similar. The main difference is that the regular 2-D waves appear at higher gas velocities and exist over a narrower range of flow conditions as the liquid viscosity increases.

*(b) High-viscosity liquids*

Wave patterns with a liquid of high viscosity, 80 cP, differ from those with a low-viscosity liquid in that the region of regular 2-D waves barely exists and in that the interface appears less roughened even when waves are present. Examples of these waves are given in figure 10. The first disturbances that are observed with increasing gas velocity are small-amplitude, small-wavelength, rather regular 2-D waves. However, with just a slight increase in gas velocity, these give way to a few large-amplitude waves with steep fronts and smooth troughs, and with spacings that can vary from a few centimeters to a meter; see figure 10(a). Occasionally, several small 2-D waves can be seen in front of the large waves. This sequence of events that accompanies the initiation of waves on a very viscous liquid is the same as had been observed some years ago by Francis (1954, 1956) in his studies of gas flow over a deep liquid.

With increasing gas flow the spacing between the waves decreases and the crests become curved; see figure 10(b). Eventually the waves become cell-like and extend only over a part of the liquid surface; see figures 10(c,d). Under these conditions the spacing is 1–2 cm.

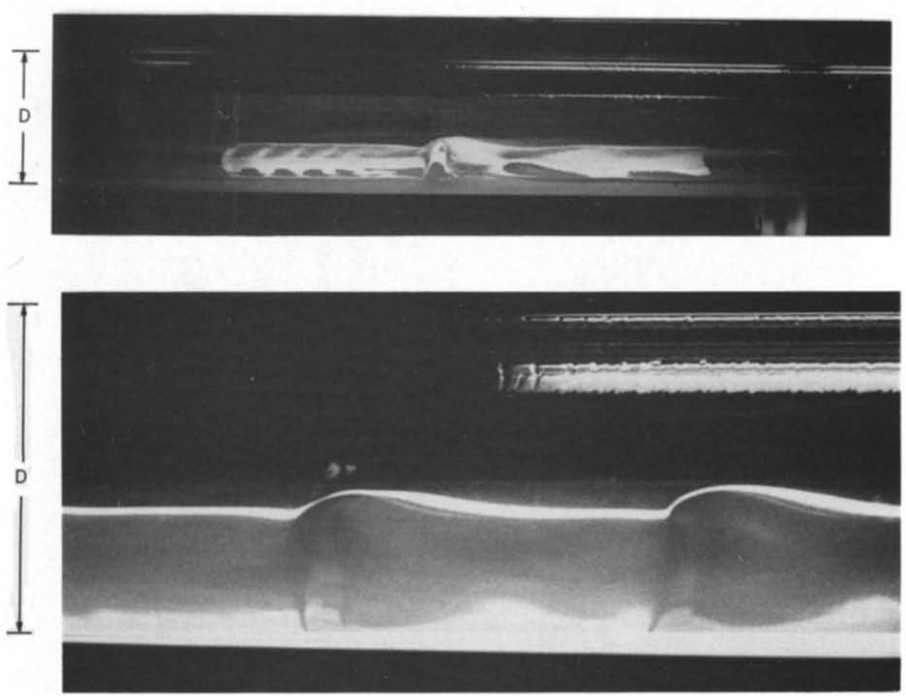


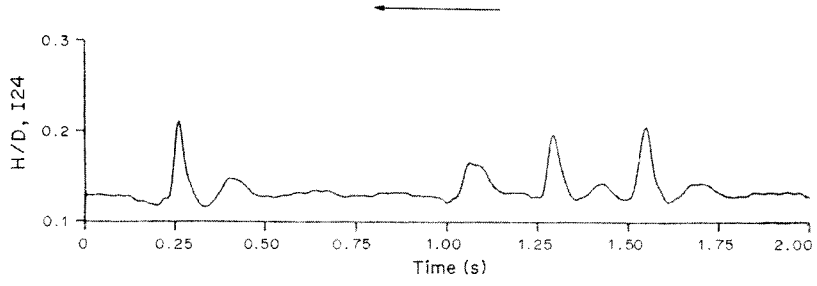


(a) $U_{GS}$ = 8.8 m/s, $\frac{f_i}{f_G}$ = 5.0

Figure 10(a)

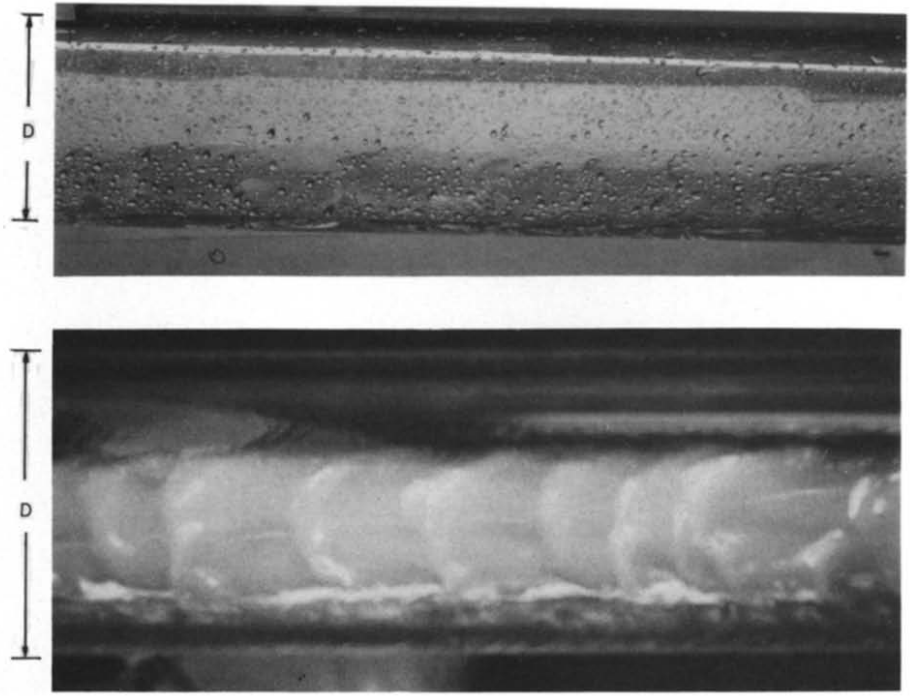


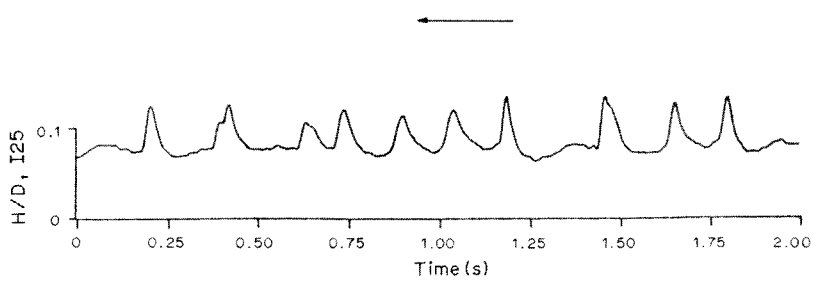


(b) $U_{GS}$ = 12.0 m/s, $\frac{f_i}{f_G}$ = 7.5

Figure 10(b)

D = 9.53 cm, $U_{LS}$ = 0.005 m/s

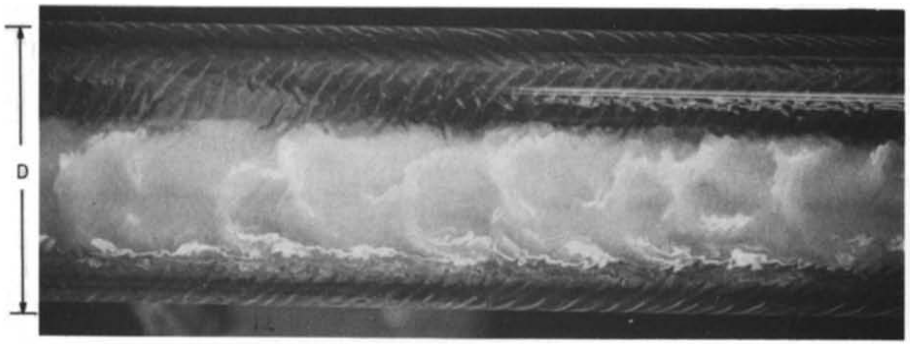


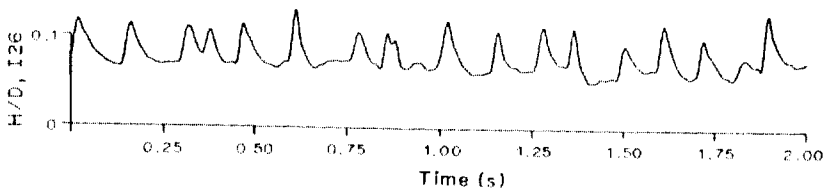


(c) $U_{GS} = 14.0\ m/s$, $\frac{f_i}{f_G} = 9.0$

Figure 10(c)

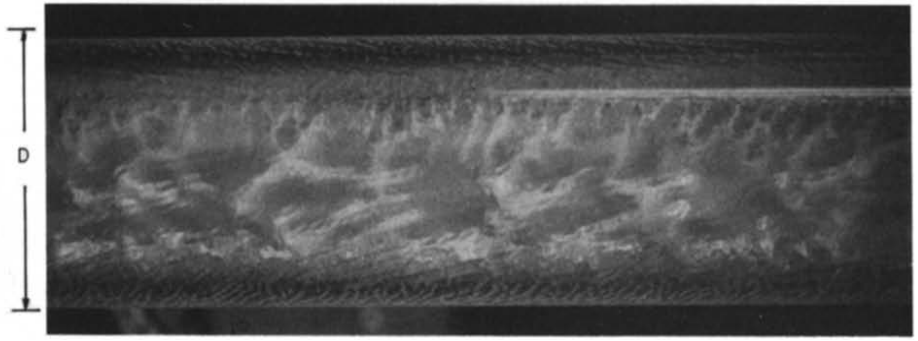


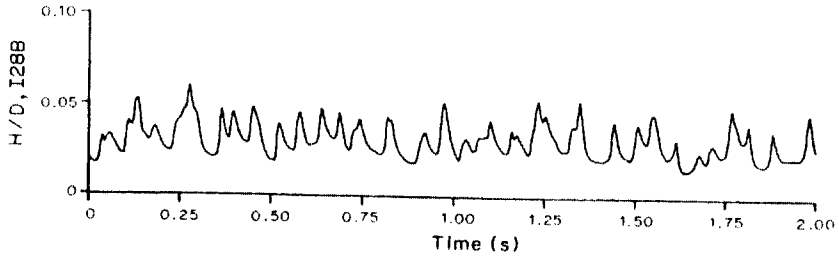


(d) $U_{GS} = 24.0\ m/s$ $\frac{f_i}{f_G} = 15.0$

Figure 10(d)

$D = 9.53\ cm$, $U_{LS} = 0.005\ m/s$

Figures 10(a–d). Large-amplitude waves in a viscous liquid.

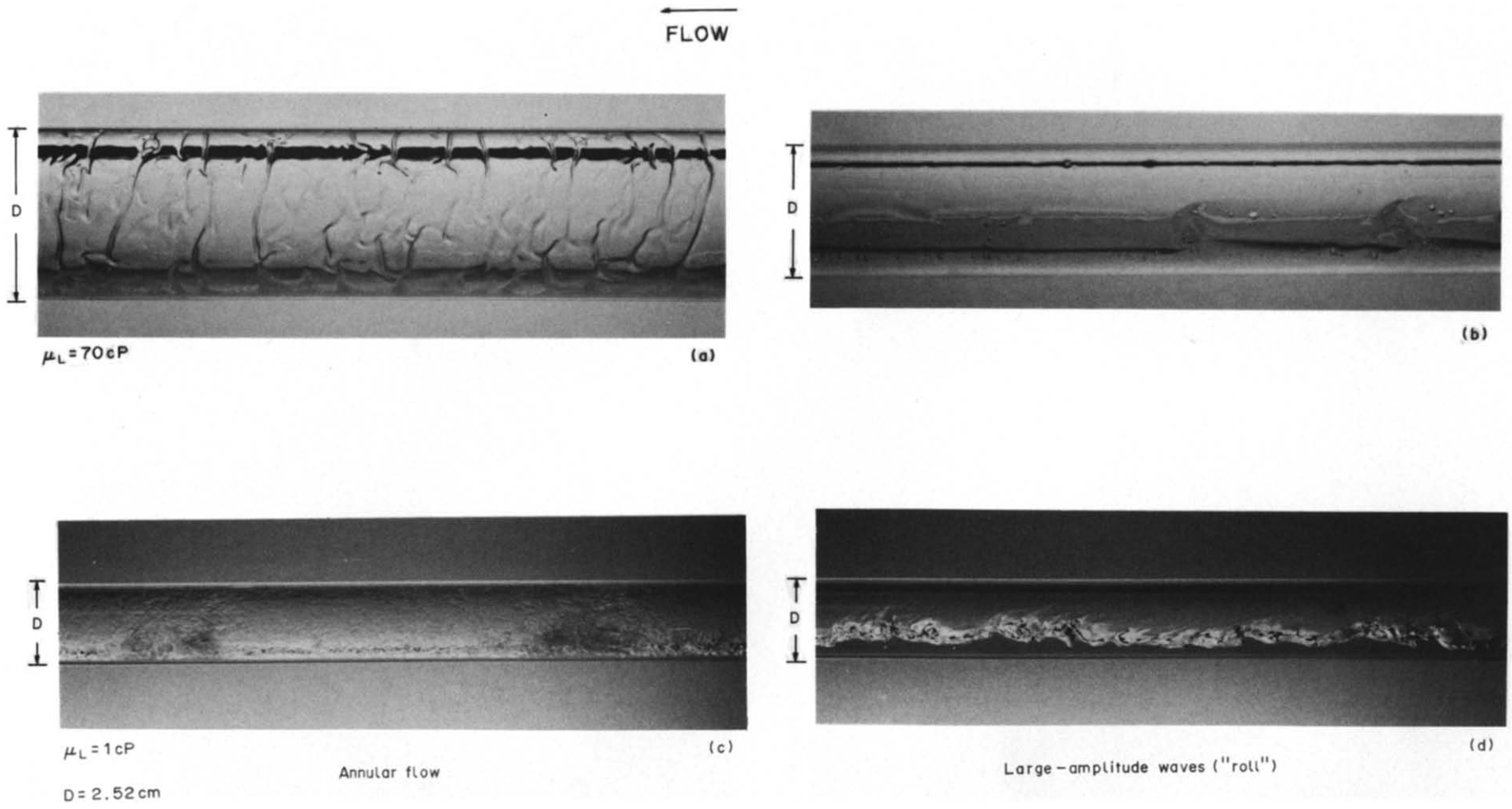


Figure 11. Annular flow and large-amplitude waves for 1 and 70 cP liquids.

As the crest becomes more curved the liquid starts to climb around the pipe circumference and atomization is initiated. The droplets formed with the 80 cP liquid appeared to be much smaller than those formed with water flows. They are thought to originate by the spewing of liquid from the crest of the large amplitude waves rather than by the removal of a wavelet, as has been suggested for water flows.

The annular flow that eventually forms at high enough gas velocities (see figure 11) has some major differences from that observed for water flows; cf. figures (11a,c). No disturbance waves were observed for the high-viscosity liquid for the range of flows studied. The waves are more broad crested and have a larger spacing. In fact, some of these waves ring around the pipe circumference. An interesting feature is that these ripples are usually oriented at an angle of $<90°$ to the flow. This suggests the possibility that a lifting force on these waves by the gas flow may be an important mechanism to counterbalance the tendency of the liquid to drain to the bottom of the pipe because of gravity.

## 5. FLOW REGIME TRANSITIONS

Maps showing the range of flow conditions for the different observed patterns are given by the curves in Mandhane-type plots in figures 12–17. The method used to detect slugs and pseudo-slugs is the same as described by Lin & Hanratty (1987). In this previous paper considerable attention was given to the transitions to annular flow, to slug flow and to pseudo-slug flow. In fact, the transitions to these regimes for water shown in figures 12 and 15 are the same as reported by Lin & Hanratty (1987). Consequently, this presentation will focus mainly on the change of wave pattern in the stratified flow regime. Three patterns are defined: 2-D regular waves, large-amplitude irregular waves and atomizing flows.

As mentioned in section 3, the flow in the pipeline was not fully developed at low gas velocities, with the consequence that hydraulic gradients existed. Experiments made under such conditions are indicated by the --- curves in figures 12–15.

It is noted from figures 12–14 that liquids of lower viscosity require a lower liquid throughput for the generation of slugs at low gas velocities. This appears to be responsible for the change in the shape of the pseudo-slug region with liquid viscosity.

The other main effect of viscosity is to increase the gas velocity required for the initiation of regular 2-D waves and to decrease the range of flow conditions for which they exist. In fact, for a 70 cP liquid (see figures 14 and 17) these regular waves are not observed at all.

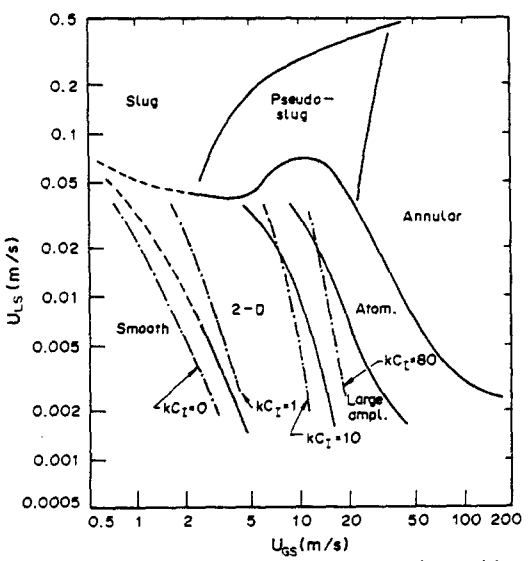


Figure 12. Flow regime map and comparison with linear theory for a 2.52 cm pipe and a 1 cP liquid: —— experimental observations; --- observations under conditions that a hydraulic gradient existed; -·-·- linear theory.

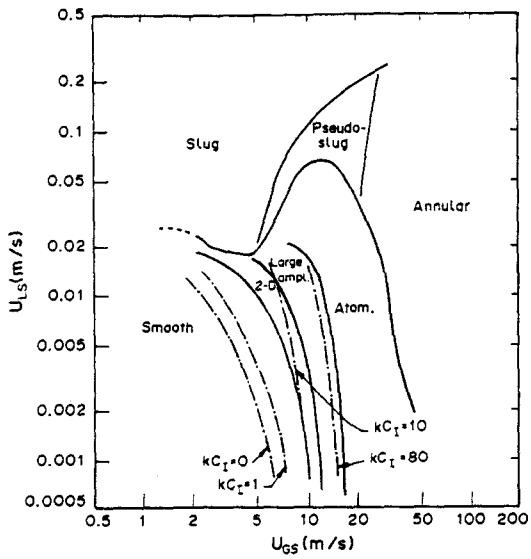


Figure 13. Flow regime map and comparison with linear theory for a 2.52 cm pipe and a 16 cP liquid: —— experimental observations; --- observations under conditions that a hydraulic gradient existed; -·-·- linear theory.

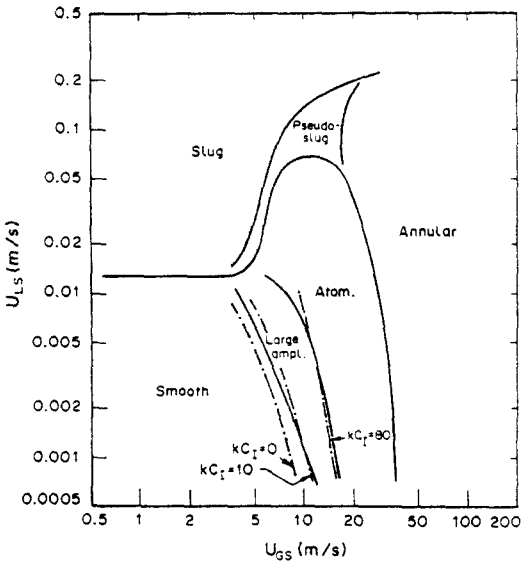


Figure 14. Flow regime map and comparison with linear theory for a 2.52 cm pipe and a 70 cP liquid: —— experimental observations; –·–·– linear theory.

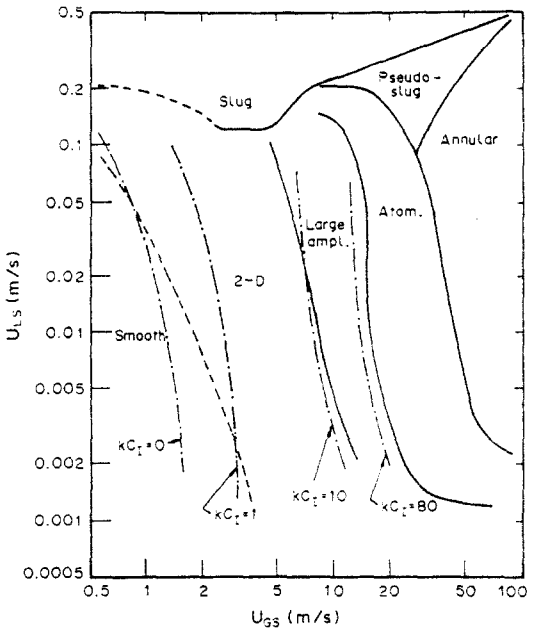


Figure 15. Flow regime map and comparison with linear theory for a 9.53 cm pipe and a 1 cP liquid: —— experimental observations; --- observations under conditions that a hydraulic gradient existed; –·–·– linear theory.

It is noted that on a Mandhane plot all of the other transitions (besides the stratified to pseudo-slug, the stratified to slug at low gas velocities, and the smooth-stratified to regular wave) are not strongly sensitive either to changes in pipe diameter or in liquid viscosity.

Figure 18 shows the same results given in figures 12 and 14 plotted as $\bar{h}/D$ vs the superficial gas velocity, where $\bar{h}$ is the height of the liquid layer at the bottom of the pipe. It is to be noted that in this type of plot (which should be less sensitive to whether the flow is fully developed) the effect

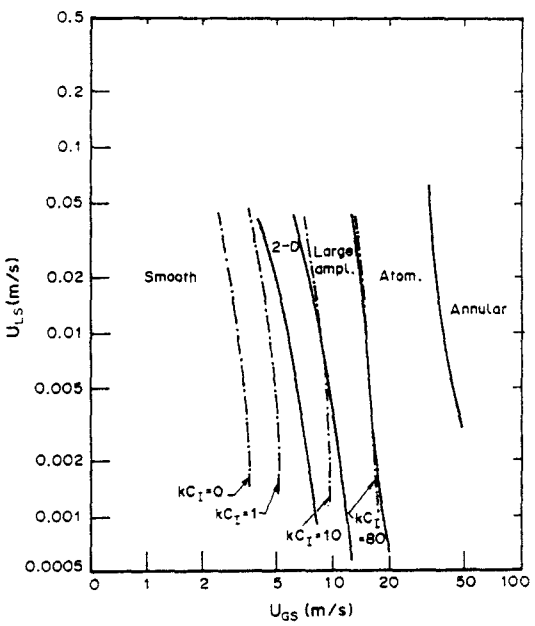


Figure 16. Flow regime map and comparison with linear theory for a 9.53 cm pipe and a 12 cP liquid: —— experimental observations; –·–·– linear theory.

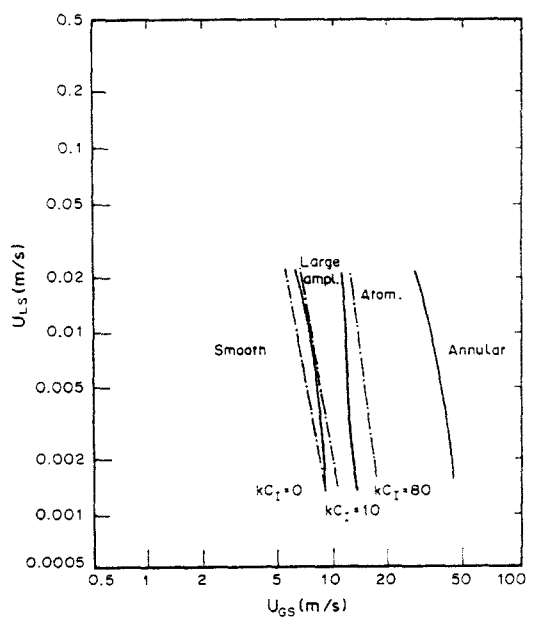


Figure 17. Flow regime map and comparison with linear theory for a 9.53 cm pipe and an 80 cP liquid: —— experimental observations; –·–·– linear theory.

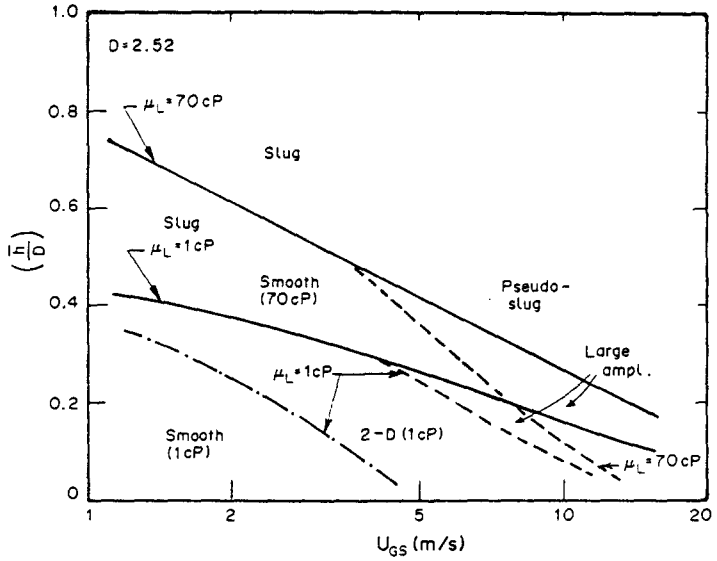


Figure 18. Liquid heights at the transitions for 1 and 70 cP liquids: —— transition to slugs and pseudo-slugs; – – – transition from 2-D waves to large-amplitude waves; –·–·– initiation of 2-D waves.

of an increase of viscosity is to make the system more stable to the initiation of slugs. A strong stabilizing effect of viscosity with respect to the initiation of regular waves and a weak stabilizing effect with respect to the initiation of large amplitude irregular waves are also noted.

## 6. COMPARISON OF WAVE TRANSITIONS TO LINEAR THEORY

Observed transitions are marked on the plots of results calculated from linear theory in figures 2–6.

Figures 2 and 3 indicate that the observed initiation of 2-D waves on low-viscosity liquids corresponds roughly with the extremum of the $C_I = 0$ curve. A more careful comparison is given in figures 12–16. It is noted that the transition is observed to occur at a larger gas velocity than is predicted (the $kC_I = 0$ curves). A possible explanation for this can be seen in figure 5, which shows that growth factor $kC_I$ maintains a relatively small value over a range of gas velocities. This could mean that better agreement would be obtained if a longer pipeline were used. Some support for this interpretation comes from the observation that the first waves appear at the outlet of the pipeline. As can be seen from figures 12–16, a somewhat better average agreement between linear stability theory and observations is obtained if $kC_I = 1\ s^{-1}$ is used as a criterion.

It is noted from figures 2 and 3 that the initiation of "large-amplitude waves corresponds roughly to the extreme of the inviscid K–H analysis for low-viscosity fluids ($\mu = 1$ cP). For a liquid with 80 cP viscosity the inviscid K–H analysis slightly underpredicts the critical gas velocity. This and the results shown in figures 5 and 6 indicate that these "large-amplitude" waves appear when pressure variations in phase with the wave height start to play an important role in determining the growth factor $kC_I$. In fact, it is noted from figure 5 that good agreement is obtained between the critical gas velocity calculated for $\hat{P}_{iI} = 0$ and observations of the critical velocity for the initiation of "large-amplitude" waves.

It is also noted that when $\hat{P}_{iR}$ is important the growth factor, $kC_I$, increases very rapidly with increasing gas velocity. Thus, the critical gas velocity should not depend very strongly on the length of the pipe. This explains why "large-amplitude" waves are initiated close to the entry.

For the case of an 80 cP liquid, shown in figure 6, the initiation of "large-amplitude" waves occurs at a gas velocity only slightly lower than the calculated critical ($kC_I = 0$). Much closer agreement is obtained if transition is defined by a growth factor of $kC_I = 10\ s^{-1}$. Figures 12–17 compare observed critical conditions for the initiation of "large-amplitude" waves with calculations from linear stability theory for $kC_I = 10\ s^{-1}$.

The initiation of atomization occurs at gas velocities approximately twice that needed for the initiation of large-amplitude waves for which the growth rates predicted by linear theory are quite large. Figures 12–17 compare observed critical gas velocities for atomization with linear theory calculations for $kC_l = 80\ s^{-1}$.

## 7. DESIGN CRITERIA

The character of the waves at the interface in stratified flow is of critical importance in determining pressure drop and hold-up and, consequently, in the development of design equations.

The experimental results presented here indicate the Mandhane *et al.* (1974) criterion for the initiation of wavy-stratified flow roughly corresponds to the initiation of large-amplitude waves. The transition to wavy-stratified flow proposed by Taitel & Dukler (1976b) corresponds to the initiation of regular 2-D waves. On the basis of the sheltering hypothesis of Jeffreys they suggested the following relation:

$$U_G \geq \left[\frac{4\nu_L(\rho_L - \rho_G)g}{s\rho_G U_L}\right]^{\frac{1}{2}}, \qquad [34]$$

where $s$ is a sheltering coefficient. This becomes meaningless for high-viscosity liquids, since regular 2-D wave are observed only for liquids with viscosity less than 20 cP. The data presented for the initiation of these waves are represented reasonably by the criterion suggested by Taitel & Dukler, except that a sheltering coefficient equal to 0.06 should be used.

As indicated in the previous discussion the inviscid K–H equation is a good first approximation for the gas velocity required to initiate irregular large-amplitude waves. We designate this as $U_{K\text{-}H}$ and define it as follows for gas–liquid flows:

$$(U_{K\text{-}H} - U_L)^2 \geq \left[\frac{k\rho}{\rho_G} + \frac{\rho_L g}{\rho_G k}\right]\tanh(k\bar{H}). \qquad [35]$$

For the range of $\bar{H}$ used in the experiments, inviscid K–H theory predicts that the minimum value of $U_{K\text{-}H}$ is attained for a wavenumber of

$$k_m = \sqrt{\frac{\rho_L g}{\sigma}}. \qquad [36]$$

For the systems studied in this research $k_m = 3.7 - 4.3\ cm^{-1}$.

A better criterion than [35] for the initiation of large-amplitude waves is obtained from [28] with $\hat{P}_{ij} = 0$. However, this is far too complicated an equation to be used for design purposes. Therefore, the following empirical equation, which takes into account the small effects of liquid height and liquid viscosity, is recommended:

$$U_{GS} = U_{K\text{-}H}\left(\frac{\theta_w}{\theta}\right)^{0.025}\left(\frac{1}{\tanh\left(\frac{k_m\bar{h}}{10}\right)}\right)^{0.1}\left(\frac{1}{\alpha}\right). \qquad [37]$$

Here $U_{K\text{-}H}$ is defined by [35] with

$$k = k_m = \sqrt{\frac{\rho_L g}{\sigma}}.$$

Dimensionless group $\theta$ was used by Taylor (1963) to account for the effects of liquid viscosity and is defined as

$$\theta = \frac{\rho_L}{\rho_G}\frac{\sigma^2}{\mu_L^2 U_G^2}. \qquad [38]$$

The term $\theta_w$ is the value of $\theta$ if the liquid is water. Velocity $U_{GS}$ is the superficial gas velocity for the initiation of large-amplitude waves and $\alpha$ is the fraction of the cross section of the pipe occupied by gas.

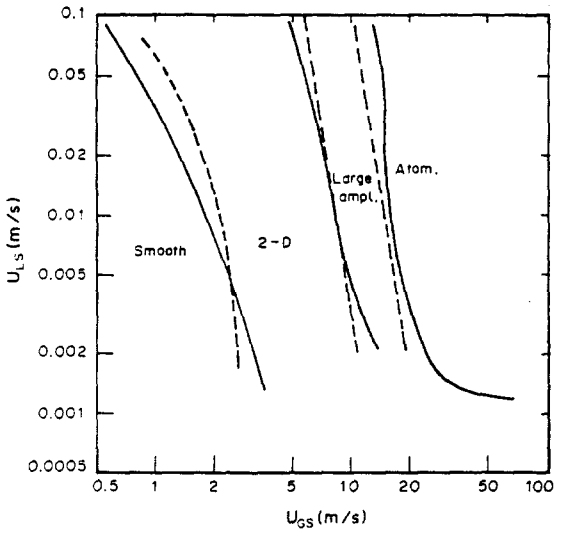


Figure 19. Comparison between experimental transitions (——) and predictions of design equations (---) for a 9.53 cm pipe and a 1 cP liquid.

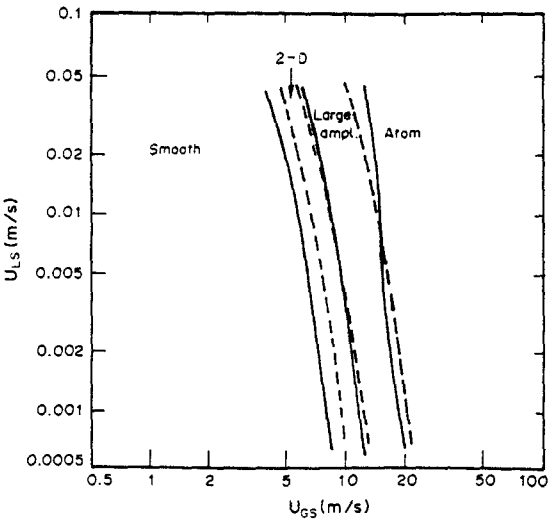


Figure 20. Comparison between experimental transitions (——) and predictions of design equations (---) for a 9.53 cm pipe and a 12 cP liquid.

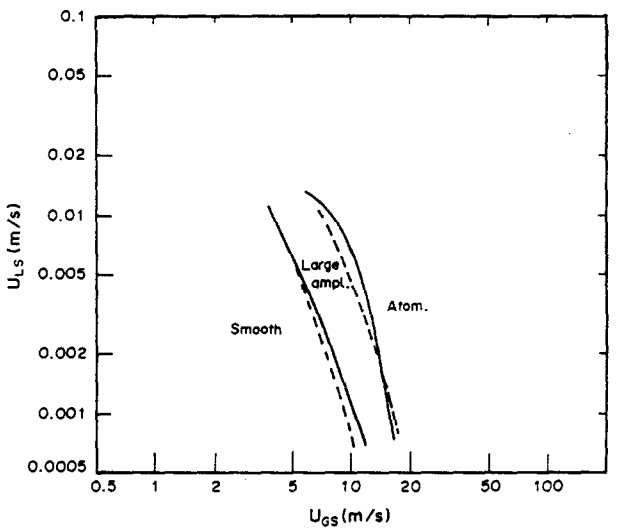


Figure 21. Comparison between experimental transitions (——) and predictions of design equations (---) for a 2.52 cm pipe and a 70 cP liquid.

An approximate criterion for the initiation of atomization is as follows:

$$U_{GS} = 1.8(U_{GS} \text{ from [37]}). \qquad [39]$$

If the conclusions presented in subsection 2(f) are correct, one would expect that the initiation of regular waves would occur at higher gas velocities for high pressures than predicted by [34]. Equations [37] and [39], however, should still be good approximations at high pressures since, according to [35], $U_{K\text{-}H} \sim (\rho_G)^{-1/2}$.

Comparisons of [34] (with $s = 0.06$), [37] and [39] with observations of the gas velocity needed to initiate regular 2-D waves, irregular "large-amplitude" waves and atomization are given in figures 19–21.

*Acknowledgements*—This work is being supported by the Shell Companies Foundation and by the Department of Energy under Grant DOE FG02-86E13556.

## NOMENCLATURE

A = Constant
B = Constant
$C$ = Wave velocity
D = Constant
$D$ = Diameter
E = Constant
$f$ = Friction factor
$h$ = Height of liquid film
$H$ = Height of gas phase
$k$ = Wavenumber
$l$ = Wavenumber, defined in [25]
$p, P$ = Local pressure in liquid and gas phases, respectively
$s$ = Sheltering coefficient
$t$ = Time
$u$ = Local velocity of liquid phase
$U_{GS}, U_{LS}$ = Superficial velocities of the gas and liquid, respectively
$U$ = Local velocity of gas phase
$U_{K\text{-}H}$ = Gas velocity, defined in [35]
$x$ = Coordinate in direction of flow
$y$ = Coordinate perpendicular to direction of flow

*Greek letters*

$\alpha$ = Void fraction
$\mu$ = Viscosity
$\nu$ = Kinematic viscosity
$\rho$ = Density
$\sigma$ = Stress
$\sigma$ = Surface tension
$\tau$ = Shear stress
$\hat{\tau}_c$ = Modified amplitude of shear stress at the interface, defined in [29]
$\phi$ = Velocity potential of liquid
$\psi$ = Function, solution of [22]

*Subscripts*

a = Quantities spatially averaged over length
G = Gas phase
i = At gas–liquid interface
I = Imaginary part
L = Liquid phase
R = Real part

*Superscripts*

$'$ = Fluctuating component of perturbation
$\bar{}$ = Time-averaged quantities
$\hat{}$ = Amplitude of fluctuating component of perturbation

## REFERENCES

ABRAMS, J. 1984 Turbulent flow over small amplitude solid waves. Ph.D. Dissertation, Univ. of Illinois, Urbana, Ill.

BAKER, O. 1954 Simultaneous flow of oil and gas. *Oil Gas J.* **53**, 185–195.

CHOW, V. T. 1959 *Open-channel Hydraulics*. McGraw-Hill, New York.

COHEN, L. S. & HANRATTY, T. J. 1965 Generation of waves in the concurrent flow of air and a liquid. *AIChE Jl* **11,** 138–144.

CRAIK, A. D. D. 1968 Wind-generated waves in contaminated liquid films. *J. Fluid Mech.* **31,** 141–161.

FRANCIS, J. R. D. 1954 Wave motions and the aerodynamic drag on a free oil surface. *Phil. Mag.* **45,** 695–702.

FRANCIS, J. R. D. 1956 Wave motions on a free oil surface. *Phil. Mag.* **1,** 685–688.

HANRATTY, T. J. 1983 Interfacial instabilities caused by air flow over a thin liquid layer. In *Waves on Fluid Interfaces.* Academic Press, New York.

HANRATTY, T. J. & ENGEN, J. M. 1957 Interaction between a turbulent air stream and a moving water surface. *AIChE Jl* **3,** 299–304.

HANRATTY, T. J. & HERSHMAN, A. 1961 Initiation of roll waves. *AIChE Jl* **7,** 488–497.

JEFFREYS, H. 1925 On the formation of water waves by wind. *Proc. R. Soc.* **107,** 189–206.

LAMB, H. 1945 *Hydrodynamics,* 6th edn. Dover, New York.

LAURINAT, J. E., HANRATTY, T. J. & DALLMAN, J. C. 1984 Pressure drop and film height measurements for annular gas–liquid flows. *Int. J. Multiphase Flow* **10,** 341–356.

LEVICH, V. G. 1962 *Physicochemical Hydrodynamics.* Prentice-Hall, Englewood Cliffs, N.J.

LIN, P. Y. & HANRATTY, T. J. 1986 Prediction of the initiation of slugs with linear stability theory. *Int. J. Multiphase Flow* **12,** 79–98.

LIN, P. Y. & HANRATTY, T. J. 1987 Effect of pipe diameter on interfacial configurations for air–water flow in horizontal pipes. *Int. J. Multiphase Flow* **13,** 549–563.

MANDHANE, J. M., GREGORY, G. A. & AZIZ, K. 1974 A flow pattern map for gas–liquid flow in horizontal pipes. *Int. J. Multiphase Flow* **1,** 537–551.

MILES, J. W. 1959 On the generation of surface waves by shear flows. Part 3. Kelvin–Helmholtz instability. *J. Fluid Mech* **6,** 583–598.

MIYA, M., WOODMANSEE, D. E. & HANRATTY, T. J. 1971 A model for roll waves in gas–liquid flow. *Chem. Engng Sci.* **26,** 1915–1931.

TAITEL, Y. & DUKLER A. E. 1976a A model for predicting flow regime transitions in horizontal and near horizontal gas–liquid flow. *AIChE Jl* **22,** 47–55.

TAITEL, Y. & DUKLER, A. E. 1976b A theoretical approach to the Lockhart–Martinelli correlation for stratified flow. *Int. J. Multiphase Flow* **2,** 591–595.

TAYLOR, G. I. 1963 Generation of ripples by wind blowing over a viscous fluid. In *The Scientific Papers of Sir G. I. Taylor, III* (Edited by BATCHELOR, G. K.), pp. 244–254. Cambridge Univ. Press, Cambs.

THORSNESS, C. B., MORRISROE, P. E. & HANRATTY, T. J. 1978 A comparison of linear theory with measurements of the variation of shear stress along a solid wave. *Chem. Engng Sci.* **33,** 579–592.

ZILKER, D. P., COOK G. W. & HANRATTY T. J. 1977 Influence of the amplitude of a solid wavy wall on a turbulent flow. Part I. Non-separated flows. *J. Fluid Mech.* **82,** 29–51.